NANO LETTERS

Letter

pubs.acs.org/NanoLett

Improved in Vitro Efficacy of Gold Nanoconstructs by Increased Loading of G-quadruplex Aptamer

Duncan Hieu M. Dam,[†] Raymond C. Lee,[†] and Teri W. Odom*[,†,‡]

[†]Department of Chemistry and [‡]Department of Materials Science and Engineering, Northwestern University, 2145 Sheridan Road, Evanston, Illinois 60208, United States

Supporting Information

ABSTRACT: This paper describes how in vitro efficacy of aptamer-loaded gold nanostars (Apt-AuNS) can be enhanced by the increased loading of a G-quadruplex homodimer AS1411 (Apt) on the AuNS surface. In a low pH buffer environment, the loading density of Apt on AuNS was increased up to 2.5 times that obtained using the conventional salt-aging process. These highly loaded AuNS nanoconstructs (*Apt-AuNS) were taken up in pancreatic cancer and fibrosarcoma cells ca. 2 times more and at faster rates compared to Apt-AuNS. When a similar number of AuNS carriers was internalized by the cancer cells, the amount of AS1411 delivered via *Apt-AuNS was effectively double that of Apt-AuNS, and *Apt-AuNS resulted in an average of 42% increase in cell death. These results suggest that increasing the loading density on AuNS could provide a simple means to improve uptake as well as *in vitro* efficacy of the nanoconstructs in cancer cells.

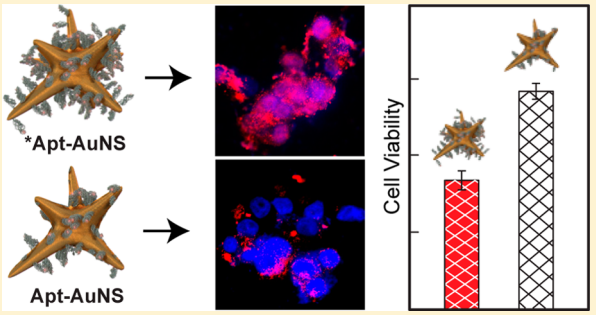

KEYWORDS: *Gold nanostars, aptamers, nucleolin, nanoconstructs, polyvalency, oligonucleotide loading*

Nanoconstructs composed of two primary components, a metal nanoparticle (NP) core and a shell of biomolecular ligands, are important in cancer diagnostics and treatment.[1−5] Among NP core materials, gold nanoparticles (AuNPs) have been the most widely studied because they can be functionalized with ligands containing terminal groups such as thiols, phosphines, and amines.[1,3,6,7] The loading of ligands on AuNPs typically relies on the self-assembly of thiolated biomolecules (oligonucleotides, antibodies, and peptides). The high density of ligands comprising the shell results in a high local concentration of biomolecules; thus, nanoconstructs often exhibit superior properties compared to the free form of the biomolecule.[8−13] For example, aptamer-loaded gold nanostars exhibited on average an increase of 20% in vitro efficacy in wide range of cancer cells compared to free aptamer drug at over 10 times the concentration.[14,15] Other work has also demonstrated that a 10-fold increase of DNA on AuNPs enhanced uptake in cancer cells by three times.[9] One hypothesis regarding how the high packing density of ligands affects the overall functionality of the nanoconstruct is polyvalency, where multiple ligands on the AuNPs can interact with multiple target receptors.[16,17]

Although ligand type and density dictate the properties of the nanoconstruct,[1] there are only a few reports on how to load oligonucleotides onto AuNPs. The most common method involves a two-day process of salt addition at high concentration (150−300 mM NaCl; pH 7.5) and an excess quantity of ligands (>5000× compared to the AuNP concentration).[1,13,18] This procedure is known as salt-aging, referred to as SALT in this paper. Because most AuNPs are stabilized with negatively charged citrate molecules,[19] micromolars of thiolated oligonucleotides are needed for nanomolars of AuNPs to displace the citrate capping layer and form stable oligonucleotide-AuNP constructs.[20] Increased packing of thiolated DNA can be achieved by adding millimolars of NaCl to help reduce charge repulsions between DNA.[20−22] Recently, a new procedure to attach single-stranded DNA (ssDNA) onto citrate-capped AuNPs used citrate buffer at pH 3.[13] For simplicity, we refer to this procedure as CIT-3. At pH 3, three DNA bases, adenine (A), cytosine (C), and thymine (T), are slightly positively charged, and the citrate-capping layer on AuNPs is partially protonated.[13,23] Protonation of the citrate layer and DNA at pH 3 reduced repulsive forces, which facilitated faster adsorption of DNA onto the AuNPs. Simultaneously, the Na^+ in the citrate buffer screened charges between the oligonucleotides to facilitate efficient packing. Overall, CIT-3 required a lower initial concentration of DNA, a lower salt concentration (10 mM), and a shorter conjugation time (10 min) compared to SALT.[13] The loading density for ssDNA, however, was comparable for both methods.[13] Previously, we used SALT to load the DNA aptamer drug AS1411 on AuNS to create nanoconstructs (Apt-AuNS) with anticancer effects.[14] AS1411 forms a G-quadruplex homodimer structure (Apt) that binds to nucleolin, a cell-surface receptor overexpressed on and within cancer cells.[24−26] Although the

Received: March 5, 2014
Revised: March 31, 2014
Published: April 1, 2014

   dx.doi.org/10.1021/nl500844m | *Nano Lett.* 2014, 14, 2843−2848

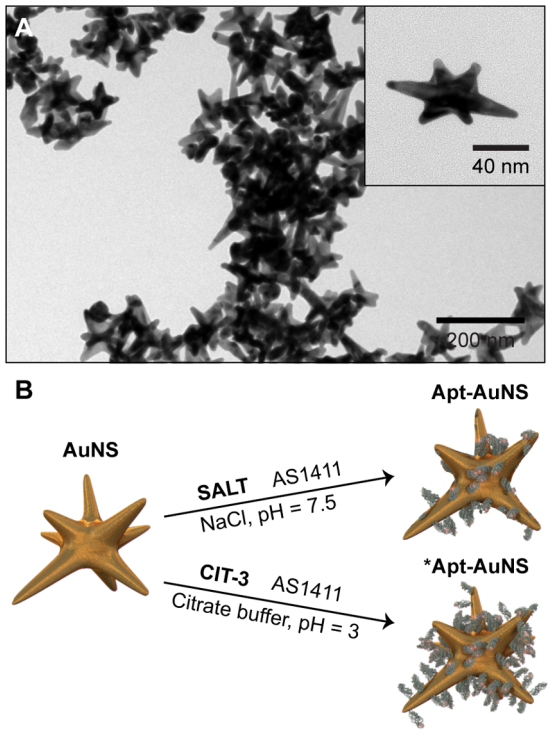

Figure 1. Preparation of AuNS nanoconstructs. (A) TEM images of AuNS synthesized by reducing $HAuCl_4$ in HEPES buffer at room temperature. (B) Synthesis of AuNS nanoconstructs using SALT (Apt-AuNS) and via CIT-3 (*Apt-AuNS).

uptake mechanism for AS1411 is not well understood, previous work suggests cellular entry through macropinocytosis after Apt binds to nucleolin.[27] We have demonstrated that the dense packing of Apt on AuNS enabled the internalization of Apt-AuNS nanoconstructs in a wide range of cancer cells, which resulted in the reduction of antiapoptotic *bcl*-2 mRNA and improved in vitro efficacy compared to the free aptamer.[14,15]

Here we report how CIT-3 can be used to load oligonucleotides with secondary structure on AuNPs at higher densities compared to SALT. We found that a G-quadruplex homodimer (Apt) could be loaded onto AuNS with a density up to 2.5× higher. This highly loaded nanoconstruct (*Apt-AuNS) was taken up by pancreatic cancer cells and fibrosarcoma cells at faster rates and with ca. twice the number compared to Apt-AuNS. We found that the increased loading of Apt on AuNS also resulted in an enhanced in vitro response. Moreover, when similar quantities of AuNS were internalized by cancer cells, but having different densities of Apt, we found that *Apt-AuNS showed on average a 42% increase in cancer cell death compared to Apt-AuNS. Because the biological activity of the aptamer drug affects many properties of the nanoconstruct, increasing the loading density on AuNS could provide a simple means to improve uptake as well as in vitro efficacy in cancer cells.

AuNS were synthesized by reducing a gold precursor ($HAuCl_4$) in 2-[4-(2-hydroxyethyl) piperazine-1-yl] ethanesulfonic acid (HEPES) buffer,[14,28] where HEPES molecules acted as both the reducing and a shape-directing agents (Figure 1A). The average hydrodynamic diameter of the synthesized AuNS was 37.1 ± 0.3 nm (Table 1). Since the AuNS were coated with HEPES, its surface charge (−33 mV) was measured to be more positive than that of citrate-capped AuNPs (−45 mV). Because of this relatively large difference in charge, AuNS can serve as a test case to determine whether CIT-3 can be used to load oligonucleotides on AuNPs besides colloidal ones capped with citrate. We first examined CIT-3 loading conditions by varying the ratio of Apt to AuNS from 5000:1 to 200:1 and the concentration of citrate buffer at pH 3 from 15 to 55 mM. Figure 1B depicts a scheme of Apt loading on the nanoconstructs through CIT-3 (*Apt-AuNS) and SALT (Apt-AuNS). The upper-limit conditions investigated for CIT-3 were similar to that used in SALT (concentration ratio of 5000:1 Apt/AuNS and 167 mM of NaCl).[14] To quantify the number of G-quadruplex homodimers on AuNS, we labeled the 5′-end of Apt with Cy5. After the AuNS core was digested in KCN, the fluorescence intensity of the released Cy5-labeled Apt was measured to determine the number of Apt on the AuNS (Supporting Information). Figure 2 shows that at lower

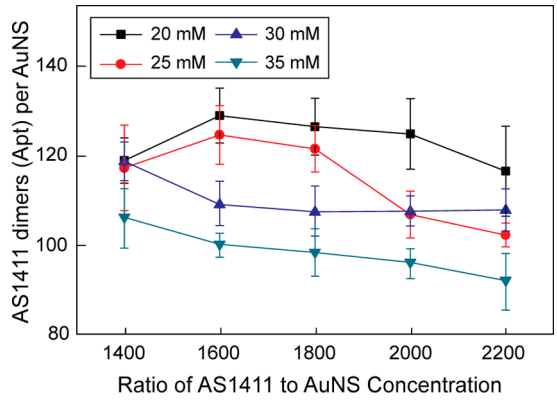

Figure 2. Optimization of CIT-3 for preparing highly loaded aptamer gold nanoconstructs. Higher loading of Apt was obtained at lower concentrations of sodium citrate buffer (20−25 mM). The concentration ratio of 1600:1 Apt/AuNS at these buffer concentrations resulted in 126 ± 6 homodimers/AuNS.

concentrations of sodium citrate buffer (20−25 mM), a higher loading of Apt was obtained. We also found that the concentration ratio of 1600:1 Apt/AuNS resulted in 126 ± 6 homodimers/AuNS for *Apt-AuNS nanoconstructs. This number was ca. 2.5-times higher than that from SALT (55 ± 3 homodimers/AuNS) (Table 1). Significantly, loading of Apt via CIT-3 was finished within 1 h, while SALT required 2 days.

To support further the observation of increased loading, we analyzed the optical properties of the nanoconstructs. The localized surface plasmon (LSP) resonance of *Apt-AuNS was red shifted by 20 nm (λ_{LSP} = 838 nm) compared to that of Apt-

Table 1. Synthetic Conditions and Characterization of AuNS Nanoconstructs

	size (nm)	LSPR peak (nm)	Apt per AuNS (dimers)	ζ-potential (mV)	conc. ratio [Apt]/[AuNS]	conc. of [Na^+] (mM)
AuNS	37.1 ± 0.3	800		−33.2 ± 2.8		
Apt-AuNS	48.5 ± 1.0	818	55 ± 3	−23.2 ± 2.4	5000:1	167
*Apt-AuNS	45.3 ± 0.5	838	126 ± 6	−29.8 ± 2.1	1600:1	75

dx.doi.org/10.1021/nl500844m | *Nano Lett.* 2014, 14, 2843−2848

AuNS (λ_{LSP} = 818 nm) (Table 1). This shift to longer wavelengths indicated that the local refractive index at the surface of the AuNS had increased, which can be explained by higher loading of Apt. Furthermore, the surface charge of *Apt-AuNS (−29.8 mV) was more negative than that of Apt−AuNS (−23.2 mV), which also confirmed an increase in Apt loading (Table 1). Our results not only confirmed that faster loading of DNA could be accomplished with CIT-3, but that this method could be extended to other adsorbed anions on AuNPs as well as oligonucleotides with secondary structure. Moreover, CIT-3 produced higher loading of a G-quadruplex Apt, although a comparable experiment with ssDNA (19-mer) showed similar loading on AuNS for CIT-3 and SALT (Supporting Information Figure S1), which is in agreement with the literature.[13] Our hypothesis is that although the adsorption of ssDNA onto AuNS is low during the initial step of SALT, ssDNA is flexible and can adopt different conformations to achieve efficient packing after 2 days. Homodimers of AS1411, however, are bulkier and are more rigid because of their G-quadruplex structure. Thus, low adsorption of Apt on AuNS using SALT did not enable efficient packing even though high concentration of salt was present to help screen charge. Because CIT-3 accelerates adsorption of DNA on AuNPs, this phenomenon may help in directing and loading AS1411 onto AuNS.

The increased loading of nontargeted DNA on colloidal AuNPs has been shown to increase uptake in cancer cells.[9] We hypothesized that *Apt-AuNS would also be internalized by cancer cells more effectively than Apt-AuNS not only because of the higher loading of Apt but also because Apt can target the cell-surface marker nucleolin.[25,29] We selected pancreatic cancer (PANC-1) and fibrosarcoma (HT-1080) cells as model systems because their tumors represent two different subcategories of cancers that lack of available treatments.[30] To evaluate uptake of the nanoconstructs, we incubated the cancer cells with 0.3 nM of Cy5-labeled *Apt-AuNS and Apt-AuNS for two different times: 2 h (t = 2 h) and 7 h (t = 7 h) at 37 °C in a 5% CO_2 environment (Supporting Information). Figure 3 depicts confocal fluorescence microscopy images of Cy5-labeled nanoconstructs (red fluorescence) that overlapped with the DAPI-stained nuclei (blue fluorescence) in both HT-1080 and PANC-1 cells. These results indicated that even after short incubation times (t = 2 h), *Apt-AuNS were internalized in much higher quantities than Apt-AuNS (Supporting Information Figure S2). After t = 7 h, the differences in the intensity of Cy5 signals between *Apt-AuNS and Apt-AuNS were even more pronounced.

To quantify the differences in fluorescence intensity, we measured the Au content of *Apt-AuNS and Apt-AuNS internalized in PANC-1 and HT-1080 cells using inductively coupled plasma mass spectrometry (ICP-MS). Using a two-dimensional (2D) projection of AuNS from transmission electron microscopy (TEM) images to estimate the volume of the particle, we converted the Au content to number of AuNS per cell (Supporting Information). We observed that at 2 and 7 h incubation times, the number of *Apt-AuNS was higher than that of Apt-AuNS in both cell types. The data strongly agreed with the qualitative confocal results. At t = 7 h, there were 15 ± 1.3 × 10^6 AuNS per cell in *Apt-AuNS treated samples of HT-1080, which was ca. 1.5× higher than that of Apt-AuNS (10 ± 0.6 × 10^6 AuNS/cell) (Figure 4A). In PANC-1 cells, the number of *Apt-AuNS per cell (68 ± 13 × 10^6) was twice that of Apt-AuNS (33 ± 3.4 × 10^6) after a 7 h incubation (Figure 4B). TEM images of cell sections revealed that the nanoconstructs were localized to the perinuclear regions and caused deformation of the nuclear membrane in both HT-1080 and PANC-1 cells (Supporting Information Figure S3). This change in nuclear phenotype because of the presence of the nanoconstructs was similar to what we observed previously in HeLa cells.[14]

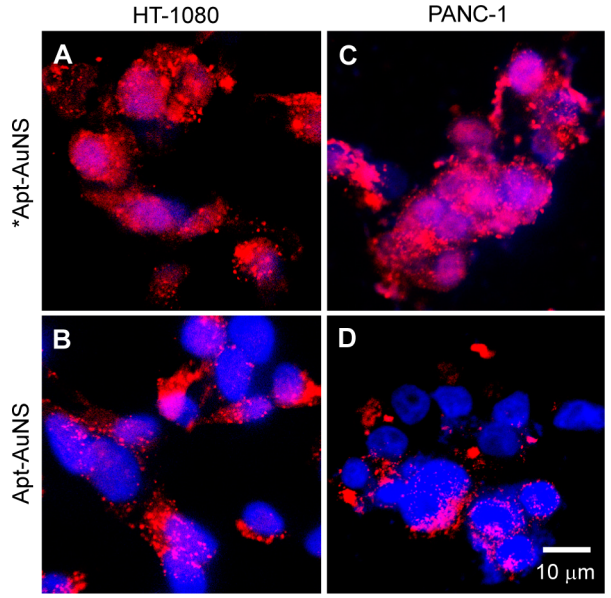

Figure 3. Confocal microscopy comparison of *Apt-AuNS and Apt-AuNS uptake after 7 h incubation in HT-1080 and PANC-1 cells. Fluorescence signal of Cy5-labeled nanoconstructs (red) in the cytoplasm and near DAPI-stained nuclei (blue) was higher in HT-1080 cells incubated with (A) *Apt-AuNS versus (B) Apt-AuNS. A similar trend was found for PANC-1 cells treated with (C) *Apt-AuNS versus (D) Apt-AuNS. The increase in Cy5 signal intensity suggests that *Apt-AuNS were internalized more efficiently than Apt-AuNS. Confocal images are 60 μm × 60 μm.

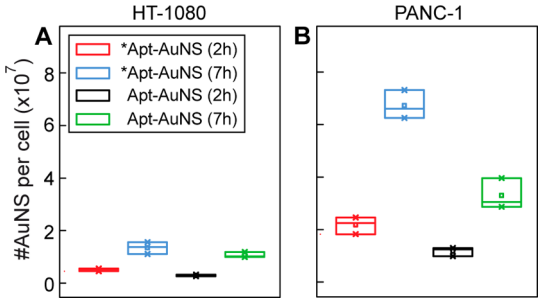

Figure 4. Quantitative uptake of nanoconstructs in fibrosarcoma and pancreatic cancer cells. (A) Number of *Apt-AuNS per HT-1080 cell was 1.5× higher than that of Apt-AuNS after 7 h incubation. (B) Number of *Apt-AuNS was twice that of Apt-AuNS per PANC-1 cell after 7 h. At both incubation times (t = 2 h and t = 7 h), the number of *Apt-AuNS was much higher than that of Apt-AuNS in HT-1080 and PANC-1 cells.

To correlate effects of nanoconstruct uptake on in vitro efficacy, we determined the amount of cell death after incubation with *Apt-AuNS and Apt-AuNS using a cell viability assay (Supporting Information). Figure 5A compares the percentage of cell death in HT-1080 at two incubation times. The percentage of cell death after a 2-h incubation with *Apt-AuNS (36%) increased by 1.5 times compared to Apt-AuNS

dx.doi.org/10.1021/nl500844m | Nano Lett. 2014, 14, 2843−2848

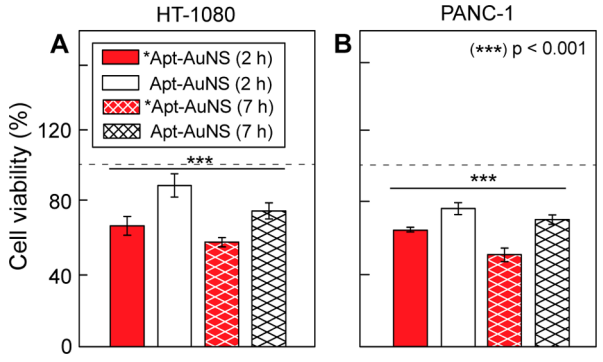

Figure 5. In vitro efficacy of AuNS nanoconstructs in HT-1080 and PANC-1 cells. (A) The percentage of cell death after a 2 h incubation increased by 1.5× with *Apt-AuNS compared to Apt-AuNS. At t = 7 h, the percentage of cell death increased by 50%. (B) The percentage of PANC-1 cell death after treatment with *Apt-AuNS increased by 42% at t = 2 h and over 65% at t = 7 h.

(14%). At t = 7 h, we observed a 50% increase in cell death: 45% with *Apt-AuNS and only 30% with Apt-AuNS. These results suggest that increased uptake can also enhance in vitro effects. A normal skin fibroblast (HS-27) was selected as a control cell line to HT-1080, since adverse effects on fibroblast cells may suggest potential toxicity of the nanoconstructs in other healthy cells. The viability assay also indicated that *Apt-AuNS and Apt-AuNS caused no negative effects in HS-27 cells (Supporting Information Figure S4A).

Figure 5B shows a similar improvement of in vitro efficacy in PANC-1 cells after treatment with *Apt-AuNS. The percentage of cell death at t = 2 h increased by 42% in *Apt-AuNS incubated PANC-1 cells (37%) compared to Apt-AuNS (26%). After a 7 h incubation, we observed greater than 65% increase of cell death with *Apt-AuNS (51%) compared to Apt-AuNS (31%). The two-way ANOVA test confirmed the significant differences (p < 0.001) in cell death number. We also assessed toxicity of both nanoconstructs in a normal mammary epithelial cell line (MCF-10A) as a control. Similar to what we observed in HS-27, only minimal cell death was observed (Supporting Information Figure S4B). Overall, we found that the in vitro efficacy of *Apt-AuNS was superior to that of Apt-AuNS.

Finally, we investigated directly the effects of higher Apt loading on the nanoconstructs by comparing the in vitro efficacy after a similar number of nanoconstructs had been internalized by cancer cells. We first determined the incubation time at which a similar amount of AuNS was taken up in HT-1080. Figure 6A,B show that Cy5-labeled *Apt-AuNS at t = 5 h and Apt-AuNS at t = 7 h have similar uptake in cancer cells, indicated by similar fluorescence intensity of Cy5 signals in confocal images and confirmed quantitatively with ICP-MS (ca. 10×10^6 AuNS/cell) (Supporting Information Figure S5). Cell viability results indicated a 44% increase of HT-1080 cell death after incubation with *Apt-AuNS (t = 5 h) (39%) compared to that with Apt-AuNS (t = 7 h) (27%) (Figure 7). With PANC-1 cells, a 3 h incubation with *Apt-AuNS resulted in numbers of nanoconstructs similar to that after 7 h incubation with Apt-AuNS (ca. 35×10^6 AuNS/cell) (Supporting Information Figure S4). These results were also confirmed qualitatively using confocal microscopy (Figure 6C,D). The percentage of cell death increased by 40% in PANC-1 cells (Figure 7). *Apt-AuNS nanoconstructs delivered 2.5× more AS1411 compared to Apt-AuNS in cancer cells, and the increased packing of drug produced in vitro efficacies higher than Apt-AuNS. Importantly,

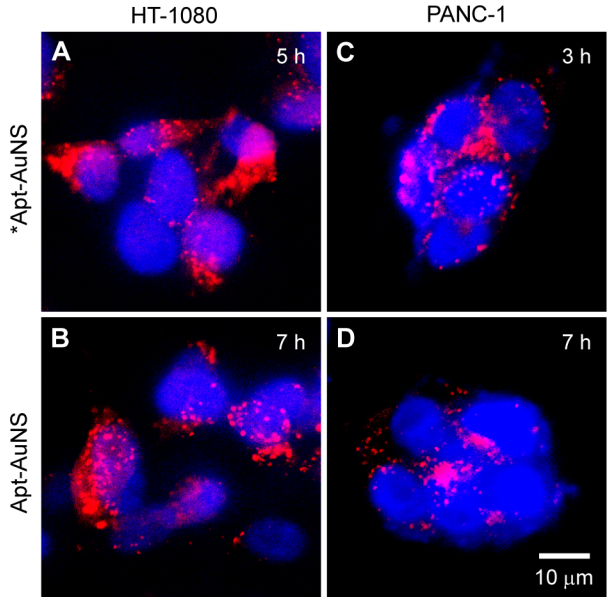

Figure 6. Uptake of similar numbers of AuNS nanoconstructs at different incubation times. Fluorescence signals of Cy5-labeled nanoconstructs (red) in the cytoplasm of HT-1080 cells were similar after treatment with (A) *Apt-AuNS (t = 5 h) versus (B) Apt-AuNS (t = 7 h). For PANC-1 cells, (C) 3 h incubation with *Apt-AuNS resulted in similar Cy5 signals to (D) 7 h incubation with Apt-AuNS. All images were collected at the same conditions.

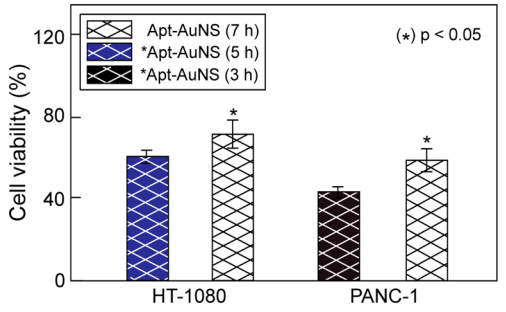

Figure 7. Enhanced in vitro efficacy of nanoconstructs from similar quantities of AuNS but different densities of Apt. (A) 44% increase of cell death in HT-1080 cells after treatment with *Apt-AuNS compared to Apt-AuNS. (B) In PANC-1 cells, a 40% increase with *Apt-AuNS was observed.

our data suggests that superior efficacy of *Apt-AuNS compared to Apt-AuNS or free AS1411 can be attributed to the potential increase of polyvalent interactions between the nanoconstructs and nucleolin in cancer cells.

In conclusion, we found that DNA aptamers having secondary structure could be loaded with higher densities and at faster rates on AuNS using a low-pH citrate buffer solution compared to the standard salt-aging procedure. This increased loading of AS1411 enhanced cellular uptake as well as in vitro efficacy of the nanoconstructs in both fibrosarcoma and pancreatic cancer cells. Importantly, our results suggest that nanoconstructs that exhibit increased polyvalency from the higher local concentrations of Apt can improve therapeutic effects. We anticipate that these results may provide a different approach to address current challenges in designing drug-loaded nanoconstructs.

dx.doi.org/10.1021/nl500844m | Nano Lett. 2014, 14, 2843−2848

■ ASSOCIATED CONTENT

Supporting Information

Experimental syntheses and characterization of AuNS, Apt-AuNS, and *Apt-AuNS; detailed procedures for quantification of Apt on AuNS, quantification of AuNS uptake in cancer cells; procedure of cell viability assays; loading of ssDNA on AuNS using SALT and CIT-3; uptake of nanoconstructs in pancreatic cancer and fibrosarcoma cells after 2 h incubation; effects of nanoconstructs in normal cells; and similar uptake of nanoconstructs. This material is available free of charge via the Internet at http://pubs.acs.org.

■ AUTHOR INFORMATION

Corresponding Author

*E-mail: todom@northwestern.edu.

Notes

The authors declare no competing financial interest.

■ ACKNOWLEDGMENTS

This work was supported by National Institutes of Health (NIH) Director's Pioneer Award DP1OD003899, the H Foundation Cancer Research Fund, the Malkin Scholar Award, and Northwestern University's Center of Cancer Nanotechnology Excellence (CCNE). We thank Kayla S. B. Culver for initial TEM images of AuNS. Confocal imaging and metal analysis were performed at the Northwestern University Quantitative Bioelemental Imaging Center supported by National Science Foundation CHE-9810378/005 and NASA Ames Research Center NNA06CB93G. Cell viability assays were carried out in the High Throughput Analysis Laboratory. UV−vis spectroscopic and fluorescence measurements were performed at the NU Keck Biophysics Facility supported by Cancer Center Support Grant (NCI CA060553). TEM experiments were conducted at the Biological Imaging Facility. The authors also thank the staff in the Developmental Therapeutic Core (DTC) for initial assistance in cell culturing and the staff in Center for Advanced Molecular Imaging (CAMI) for creating AuNS cartoon.

■ REFERENCES

(1) Giljohann, D. A.; Seferos, D. S.; Daniel, W. L.; Massich, M. D.; Patel, P. C.; Mirkin, C. A. Gold nanoparticles for biology and medicine. *Angew. Chem., Int. Ed.* **2010**, *49*, 3280−94.

(2) Liao, H. W.; Nehl, C. L.; Hafner, J. H. Biomedical applications of plasmon resonant metal nanoparticles. *Nanomedicine-U.K.* **2006**, *1*, 201−208.

(3) Hu, M.; Chen, J. Y.; Li, Z. Y.; Au, L.; Hartland, G. V.; Li, X. D.; Marquez, M.; Xia, Y. N. Gold nanostructures: engineering their plasmonic properties for biomedical applications. *Chem. Soc. Rev.* **2006**, *35*, 1084−1094.

(4) Dykman, L.; Khlebtsov, N. Gold nanoparticles in biomedical applications: recent advances and perspectives. *Chem. Soc. Rev.* **2012**, *41*, 2256−2282.

(5) Albanese, A.; Tang, P. S.; Chan, W. C. W. The Effect of Nanoparticle Size, Shape, and Surface Chemistry on Biological Systems. *Annu. Rev. Biomed Eng.* **2012**, *14*, 1−16.

(6) Herne, T. M.; Tarlov, M. J. Characterization of DNA probes immobilized on gold surfaces. *J. Am. Chem. Soc.* **1997**, *119*, 8916−8920.

(7) Chou, L. Y.; Zagorovsky, K.; Chan, W. C. DNA assembly of nanoparticle superstructures for controlled biological delivery and elimination. *Nat. Nanotechnol.* **2014**, *9*, 148−55.

(8) Agasti, S. S.; Chompoosor, A.; You, C. C.; Ghosh, P.; Kim, C. K.; Rotello, V. M. Photoregulated Release of Caged Anticancer Drugs from Gold Nanoparticles. *J. Am. Chem. Soc.* **2009**, *131*, 5728−5730.

(9) Giljohann, D. A.; Seferos, D. S.; Patel, P. C.; Millstone, J. E.; Rosi, N. L.; Mirkin, C. A. Oligonucleotide loading determines cellular uptake of DNA-modified gold nanoparticles. *Nano Lett.* **2007**, *7*, 3818−21.

(10) Huang, C. C.; Huang, Y. F.; Cao, Z. H.; Tan, W. H.; Chang, H. T. Aptamer-modified gold nanoparticles for colorimetric determination of platelet-derived growth factors and their receptors. *Anal. Chem.* **2005**, *77*, 5735−5741.

(11) Huang, Y. F.; Sefah, K.; Bamrungsap, S.; Chang, H. T.; Tan, W. Selective Photothermal Therapy for Mixed Cancer Cells Using Aptamer-Conjugated Nanorods. *Langmuir* **2008**, *24*, 11860−11865.

(12) Rosi, N. L.; Mirkin, C. A. Nanostructures in biodiagnostics. *Chem. Rev.* **2005**, *105*, 1547−62.

(13) Zhang, X.; Servos, M. R.; Liu, J. Instantaneous and quantitative functionalization of gold nanoparticles with thiolated DNA using a pH-assisted and surfactant-free route. *J. Am. Chem. Soc.* **2012**, *134*, 7266−9.

(14) Dam, D. H.; Lee, J. H.; Sisco, P. N.; Co, D. T.; Zhang, M.; Wasielewski, M. R.; Odom, T. W. Direct observation of nanoparticle-cancer cell nucleus interactions. *ACS Nano* **2012**, *6*, 3318−26.

(15) Dam, D. H.; Culver, K. S.; Odom, T. W. Grafting Aptamers onto Gold Nanostars Increases in Vitro Efficacy in a Wide Range of Cancer Cell Types. *Mol. Pharmaceutics* **2014**, *11*, 580−587.

(16) Mammen, M.; Choi, S. K.; Whitesides, G. M. Polyvalent interactions in biological systems: Implications for design and use of multivalent ligands and inhibitors. *Angew. Chem., Int. Ed.* **1998**, *37*, 2755−2794.

(17) Cutler, J. I.; Zhang, K.; Zheng, D.; Auyeung, E.; Prigodich, A. E.; Mirkin, C. A. Polyvalent nucleic acid nanostructures. *J. Am. Chem. Soc.* **2011**, *133*, 9254−7.

(18) Liu, J.; Lu, Y. A colorimetric lead biosensor using DNAzyme-directed assembly of gold nanoparticles. *J. Am. Chem. Soc.* **2003**, *125*, 6642−3.

(19) Jana, N. R.; Gearheart, L.; Murphy, C. J. Seeding growth for size control of 5−40 nm diameter gold nanoparticles. *Langmuir* **2001**, *17*, 6782−6786.

(20) Elghanian, R.; Storhoff, J. J.; Mucic, R. C.; Letsinger, R. L.; Mirkin, C. A. Selective colorimetric detection of polynucleotides based on the distance-dependent optical properties of gold nanoparticles. *Science* **1997**, *277*, 1078−1081.

(21) Mucic, R. C.; Storhoff, J. J.; Mirkin, C. A.; Letsinger, R. L. DNA-directed synthesis of binary nanoparticle network materials. *J. Am. Chem. Soc.* **1998**, *120*, 12674−12675.

(22) Cutler, J. I.; Auyeung, E.; Mirkin, C. A. Spherical Nucleic Acids. *J. Am. Chem. Soc.* **2012**, *134*, 1376−1391.

(23) Zhang, X.; Liu, B.; Dave, N.; Servos, M. R.; Liu, J. Instantaneous attachment of an ultrahigh density of nonthiolated DNA to gold nanoparticles and its applications. *Langmuir* **2012**, *28*, 17053−60.

(24) Bates, P. J.; Laber, D. A.; Miller, D. M.; Thomas, S. D.; Trent, J. O. Discovery and development of the G-rich oligonucleotide AS1411 as a novel treatment for cancer. *Exp Mol. Pathol* **2009**, *86*, 151−164.

(25) Christian, S.; Pilch, J.; Akerman, M. E.; Porkka, K.; Laakkonen, P.; Ruoslahti, E. Nucleolin expressed at the cell surface is a marker of endothelial cells in angiogenic blood vessels. *J. Cell Biol.* **2003**, *163*, 871−878.

(26) Hovanessian, A. G.; Soundaramourty, C.; El Khoury, D.; Nondier, I.; Svab, J.; Krust, B., Surface Expressed Nucleolin Is Constantly Induced in Tumor Cells to Mediate Calcium-Dependent Ligand Internalization. *PLoS One* **2010**, *5*.

(27) Reyes-Reyes, E. M.; Teng, Y.; Bates, P. J. A New Paradigm for Aptamer Therapeutic AS1411 Action: Uptake by Macropinocytosis and Its Stimulation by a Nucleolin-Dependent Mechanism. *Cancer Res.* **2010**, *70*, 8617−8629.

(28) Xie, J. P.; Lee, J. Y.; Wang, D. I. C. Seedless, surfactantless, high-yield synthesis of branched gold nanocrystals in HEPES buffer solution. *Chem. Mater.* **2007**, *19*, 2823−2830.

(29) Girvan, A. C.; Teng, Y.; Casson, L. K.; Thomas, S. D.; Juliger, S.; Ball, M. W.; Klein, J. B.; Pierce, W. M., Jr.; Barve, S. S.; Bates, P. J. AGRO100 inhibits activation of nuclear factor-kappaB (NF-kappaB) by forming a complex with NF-kappaB essential modulator (NEMO) and nucleolin. *Mol. Cancer Ther.* **2006**, *5*, 1790−9.
(30) Li, J.; Wientjes, M. G.; Au, J. L. Pancreatic cancer: pathobiology, treatment options, and drug delivery. *AAPS J.* **2010**, *12*, 223−32.